INVESTIGATION OF PROCESS PARAMETERS ON THE DISTRIBUTION OF THE SPECIFIC RESISTIVITY IN GA-DOPED CZ-CRYSTALS

F. Mosel[1], K.Hess[1], M. Trempa[2], J. Friedrich[2]
[1] PVA Crystal Growing Sytems GmbH, Im Westpark 10-12, 35435 Wettenberg, Germany
[2]Fraunhofer-Institut für Integrierte Systeme IISB, Schottkystraße 10, 91058 Erlangen, Germany
e-mail: frank.mosel@pvatepla.com
tel: +49 64168690-125, fax: +49 64168690-822

ABSTRACT: Light induced degradation (LID) which is based on a defect state of a boron atom with two oxygen atoms in Czochralski-grown crystals (BO-LID) reduces the bulk lifetime and hence the energy conversion efficiency of solar cells upon illumination. This boron-oxygen complex forms during the cooling process of the crystal. Gallium has replaced boron as doping element because it shows negligible BO-related degradation. However, as a doping element, gallium has two severe disadvantages. Firstly, a small distribution coefficient resulting in a highly inhomogeneous resistivity distribution, which means a significant reduction in the yield of substrate material in a specified resistivity range. Secondly, the hardly reproducible adjustment of the specific resistivity in Ga-doped Cz-crystals due to evaporation phenomena of gallium species. We have examined the influence of Cz-process parameters on the evaporation behavior of gallium during the crystal growth of silicon crystals in the resistivity range of interest for solar cells. We will show here our main results.
Keywords: resistivity distribution, gallium-doping, LID, Czochralski process, evaporation

1 INTRODUCTION

The fact that p-type solar cells were only produced on boron-doped wafers until recently is due to the favorable incorporation behavior of boron during the growth of silicon crystals by the Czochralski (Cz) technique. The boron distribution coefficient of k=0.8 means that boron is incorporated into the solidifying crystal with almost the same concentration as the boron concentration in the melt. Thus, a relatively uniform dopant distribution over the crystal length can be achieved. However, a disadvantage of the solar cells whose base is boron-doped is the light-induced degradation (LID). The mechanism that triggers the degradation is a boron-oxygen correlated defect. During the cooling process of the crystal, a substitutionally incorporated boron atom (B_S) combines with a mobile oxygen dimer (O_{2i}). In its ground state, this complex is a deep donor [1], which acts as a trap for minority carriers and not as a recombination center. Under the influence of light, which is equivalent to charge carrier injection, this B_SO_{2i} complex binds an electron and transforms to one of two possible shallow acceptor states. These two acceptor states result in rapid (FRC: fast forming recombination center) and slow (SRC: slow forming recombination center) formation of the BO complex that induces LID. Since the simultaneous presence of boron and oxygen is a prerequisite for the BO complex, there are various possibilities to reduce or avoid LID. Floating zone grown silicon mono crystals are almost free of oxygen. This production method is expensive compared to Cz-technology and is limited in terms of crystal diameter. An alternative growth technology is the use of a magnetic field during the Cz-process (MCz method). A constant magnetic field dampens the melt convection and thus reduces the oxygen incorporation into the crystal. Yet, this method also requires a high investment for the superconducting magnet.
The simplest method is the substitution of boron by another group III element. Since neither aluminum nor indium are alternative doping elements, gallium is the only possible candidate. Both former mentioned elements also form A_SO_2 complexes (A is either B, Al, Ga, In), of which the AlO complex shows strong recombination activity. Indium has an ionization energy of Ev +0.16eV, i.e. at room temperature only about 50% of the substitutionally incorporated indium is ionized. The non-ionized indium acts as a recombination path [2]. This leaves Ga as the only alternative for substituting boron in Cz monocrystals.
We have determined that, in contrast to boron-doped crystals, the expected resistivity distributions in gallium-doped crystals did not match those measured on the grown crystals. Fig.1 shows the axial resistivity distribution of a boron doped crystal as expected before growth (dashed green line) and measured on the surface of the crystal after growth (data). With the exception of the first two measuring points, there is a good accordance. The two outliers at the beginning of the boron-doped crystal are due to compensation of thermal donors, which often occurs at the beginning of the crystal. The red line is obtained by a least squares fit to the data. Fig.2 shows the same plot for a gallium-doped crystal. A significant deviation from the expected (green line) to the measured data is evident.
To clarify this situation we investigated the evaporation behavior of gallium during the Cz-process. We compared the results of electrical characterization with the chemical content of Ga-doped samples, measured by means ICP-MS[1].

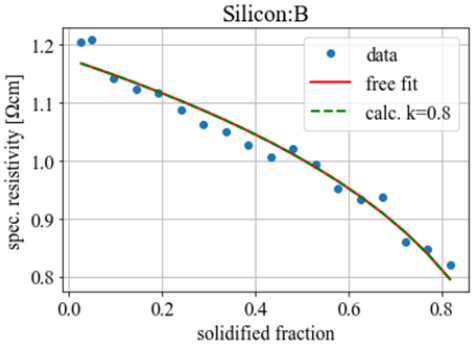

Figure 1: Axial distribution of the specific resistivity in a boron-doped Cz-crystal

[1] Fraunhofer-Center für Silizium-Photovoltaik CSP

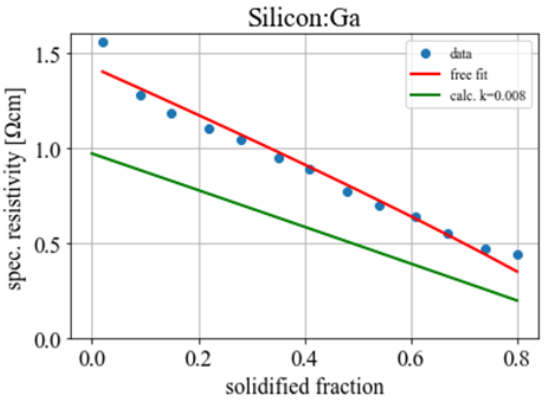

Figure 2: Axial distribution of the specific resistivity in a gallium-doped Cz-crystal

2 EXPERIMENTAL APPROACH

2.1 Overview

The crystal growth experiments presented in this paper were performed in a Cz-puller from PVA Crystal Growing Systems GmbH. A growth configuration for 26-inch crucibles was used. All samples examined in this work were grown from solar-grade polysilicon.
In the first step, the evaporation behavior of gallium during the melting phase of the charged silicon was examined. It turned out that under the test conditions during the melting phase there was no noticeable loss of Ga from the melt. In further crystal growth experiments, the evaporation was investigated under different growth conditions mainly with respect to the inert gas flow and furnace pressure. The electronic properties in the samples measured by means of Hall-effect were compared with the chemical contents of the doping elements. The results are summarized in Chapter 2.4. For completeness, we also studied the evaporation rates of aluminum and indium under standard process conditions.

2.2 Evaporation behavior of Ga during the melting phase

Two different doping methods were used to investigate the evaporation behavior of the weighed quantity of gallium during the melting phase of the polysilicon. The gallium was added to the silicon charge both in a closed silicon container (Fig.3) and unprotected as beads (Fig.4). Fig.5 shows the silicon container with its cap.

Figure 3: Ga embedded in a closed silicon container surrounded by silicon chunks

Figure 4: Ga beads surrounded by silicon chunks

Fig.6 shows the closed Si-container just before the charge was completely melted.

Figure 5: Silicon container

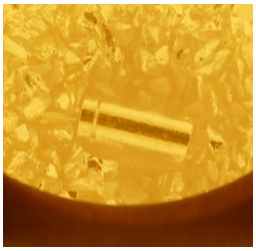

Figure 6: Silicon container during melting phase

The initial process conditions were identical for both experiments. 40 kg of polysilicon were melted, the calculated initial concentration of gallium in the melt was $4.2*10^{18}$ at/cm^3. The ratio of the free melt surface A to the melt volume V was A/V=0.18 cm^{-1}.The Ar flow rate was 30 l/min, the furnace pressure 20 mbar. The melting phase lasted 5 hours, the time gap of the melt until the sample was withdrawn from the melt was 2.5 hours. Fig 7 shows an example of the crystallized sample used for characterization.

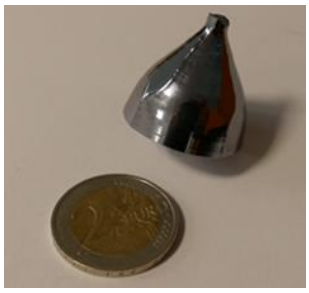

Figure 7: Si-sample and 2 € coin

The expected Ga-concentration in the sample without evaporation was $3.4*10^{16}$ at/cm^3, assuming a segregation coefficient of k=0.008. The results of the ICP measurements of the Ga-content in the two samples are given in Tab.I. Both measurements gave identical values within the framework of the standard deviation (SD). At this point it can be stated that the melting phase seems not to be a critical process phase concerning the loss of gallium which is in contradiction to the work of Hoshikawa et al. [3].

Table I: ICP-MS results of experiment chap. 2.2

	atoms/cm^3 sample Fig.3	atoms/cm^3 sample Fig.4
Gallium	$3.98*10^{16}$	$4.00*10^{16}$
SD	$1.39*10^{15}$	$1.35*10^{15}$
LOD	$2.08*10^{11}$	$1.84*10^{11}$

2.3 Evaporation behavior under process conditions:

The evaporation of volatile elements is represented by a first-order kinetic reaction, i.e. by eq.(1)

$$-\frac{dC}{C} = \gamma \frac{A}{V} dt \quad or \quad ln\left(\frac{C_t}{C_0}\right) = -\gamma \frac{A}{V} t \qquad (1)$$

where C_t, C_0, γ, A, V, t denote the actual doping element concentration [at/cm^3], initial doping element

concentration [at/cm^3], evaporation rate constant [cm/s], free melt surface [cm^2], melt volume [cm^3] and process time [s], respectively.

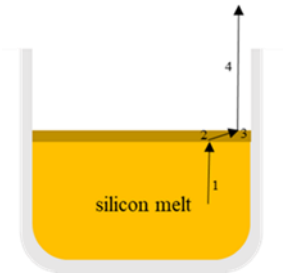

Figure 8: Sketched sequence of evaporation

Evaporation takes place in four sequential steps, which are outlined in Fig.8: 1) transport of the doping element or the oxygen compound of the doping element in the melt volume to the boundary layer, 2) transport through the melt/gas boundary layer, 3) physical evaporation process, 4) removal through the gas phase. The time dependence of the evaporation process results from the four sub steps. The transport in the melt volume is dominated by the convection phenomena in the melt volume. The transport in the boundary layer is determined by convection and diffusion of the solute. The chemical evaporation process can be described by the Hertz-Knudsen equation [4]. The transport through the gas phase is essentially influenced by the gas flow and chamber pressure.
It seems practically impossible to describe the totality of the mentioned transport processes of evaporation as a function of the crystal growth process in a manageable model. Therefore, an attempt was made to provide a tool for predicting the dopant incorporation and the resulting specific resistivity by means of numerical fit calculations on measured data of the specific resistivity (2.3.2).

2.3.1 Determination of the evaporation rate using a 2-point measurement method

For the measurement of the evaporation rates two samples were grown according to fig.9. After the first sample a second one was withdrawn from the melt after a time gap between 14 and 22 hours. Then the final crystal growth process followed.

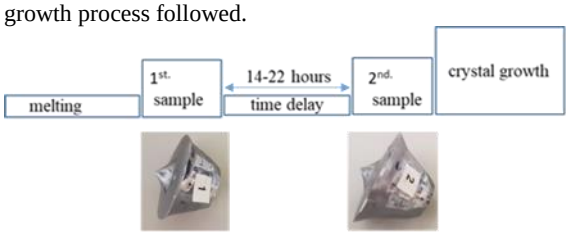

Figure 9: Time schedule of the experiments

The main process conditions for the different evaporation experiments are given in the legend of Fig.10. The diagram shows the evaporation rates determined for gallium in silicon melt under the applied process conditions plotted versus the initial Ga concentration in the melt. With the exception of the experiments under increased and reduced argon pressure an average evaporation coefficient of 3-4*10^{-5} cm/s for Ga under the applied process conditions is applicable. However, the values determined from two measurements can only be evaluated as static reference points. Fig.11 is intended to illustrate the pressure dependence of the evaporation coefficient of gallium in a silicon melt. At this point, it should be expressly noted that the silicon melt was hold in a silica crucible as a source of oxygen.

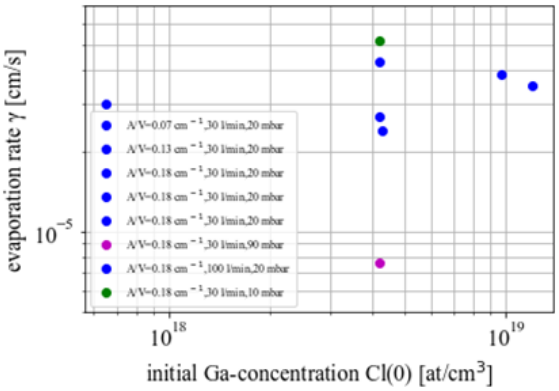

Figure 10: Overview of the evaporation coefficients γ [cm/s] of Ga in silicon melt according equation (1)

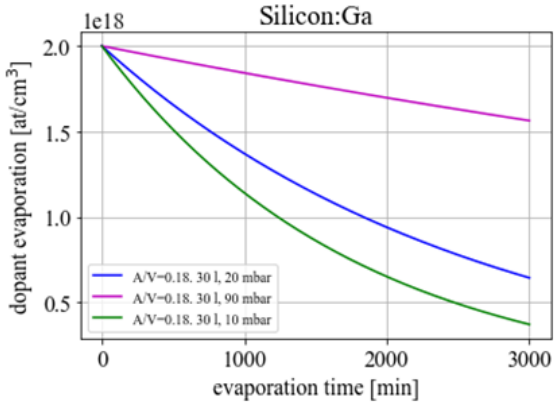

Figure 11: Evaporation of Ga in silicon melt for different gas pressures (Ar) in the process chamber, the blue line represents a mean value of 3.5*10^{-5} cm/s.

For the sake of completeness, the evaporation rates of aluminum and indium in a silicon melt were also determined and compared with the evaporation rate of gallium. Fig.12 shows the calculated loss of the different elements versus the time of the melt in the silica crucible.

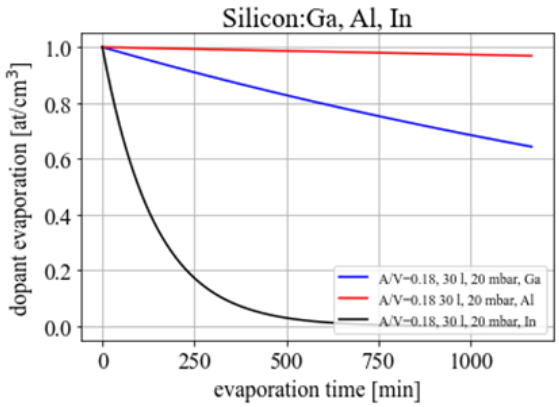

Figure 12: Estimated evaporation of group III elements in silicon melt versus time

2.3.2 Determination of the evaporation rate by least squares fitting of the extended Scheil equation

The axial dopant distribution C_S in a Cz-crystal can be

described by the directional solidification model known as Scheil equation eq.(2). The corresponding concentration of the dopant in the melt is given by eq.(4).

$$C_S = kC_l(0)(1-g)^{(k-1)} \quad (2)$$

The relationship between the concentrations in the crystal C_S and in the melt volume C_l is given by the segregation coefficient k: eq.(3).

$$\frac{C_S}{C_l} = k \quad (3)$$

$$C_l = C_l(0)(1-g)^{(k-1)} \quad (4)$$

The model describes the segregation of dopants that only take part in the melt-crystal phase transition (closed system). This assumption is entirely justified for dopants that have a negligible vapor pressure in the silicon melt. Strictly speaking, the Scheil equation applies in a conservative, closed melt/crystal system without exchange of the dissolved doping element with the environment. This idealized situation cannot be applied to volatile doping elements, which show a noticeable evaporation behavior under process conditions.
Nevertheless, there are various approaches in literature [5,6] to describe the evaporation behavior of volatile dopants by extending the Scheil equation. In our case we have expanded the exponent in the equation by a term γ_{fit}/v eq.(5). Here γ_{fit} is an expression describing the evaporation coefficient and v is the growth rate. This modified Scheil equation, takes into account the evaporation through a modified evaporation coefficient γ_{fit} and the process dynamics through the growth rate v.

$$C_l = C_l(0)(1-g)^{\left(k-1+\frac{\gamma_{fit}}{v}\right)} \quad (5)$$

The evaporation rate is influenced by a large number of process parameters, such as the concentration of the doping element in the melt, the process gas conditions (pressure and flow), the oxygen concentration in the melt and thus also the hydrodynamic conditions and the quality of the crucible, the ratio of free melt surface to melt volume A/V and many other secondary process conditions, all dependent on the nature of the Cz-process.
Fig.13 - Fig.15 show the axial resistivity distributions for some Ga-doped silicon crystals grown under identical process gas conditions. The main growth parameters are given in Tab.II. With the exception of Fig.15, the expected resistivity distributions shown as green lines are significantly lower than the data measured on the surface of the as grown crystal (Fig.13 and Fig.14). This means that the amount of gallium was not sufficient to achieve the target resistivity. The deviations were mainly caused by the evaporation of gallium from the silicon melt in the silica crucible.

Table II: Main growth parameters of crystal growth experiments, shown in Fig.13 – Fig.15

Si:Ga	$C_l(0)$ [at/cm3]	target resistvity [Ωcm] at start of body	drift mobility μ_D [$cm^2/(Vs)$], used in eq.(6)	A/V at process start	process gas
Fig.13	$1.8*10^{18}$	1.00	410	0.07	30 l/min, 20 mbar
Fig.14	$4.2*10^{18}$	0.50	410	0.13	30 l/min, 20 mbar
Fig.15	$4.4*10^{18}$	0.50	350	0.1	30 l/min, 20 mbar

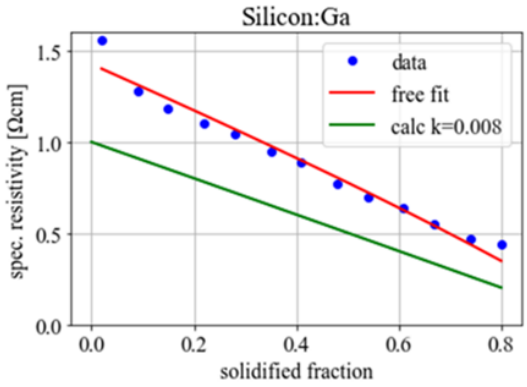

Figure 13: Axial distribution of the specific resistivity in a Ga-doped silicon crystal versus the solidified fraction

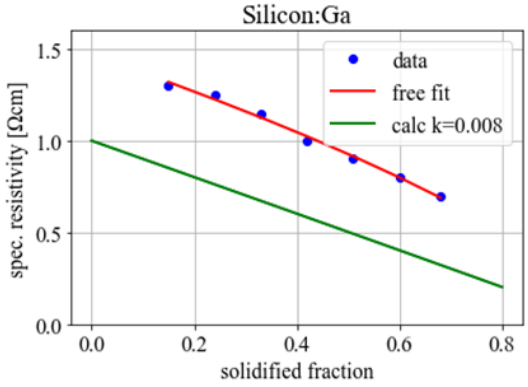

Figure 14: Axial distribution of the specific resistivity in a Ga-doped silicon crystal versus the solidified fraction

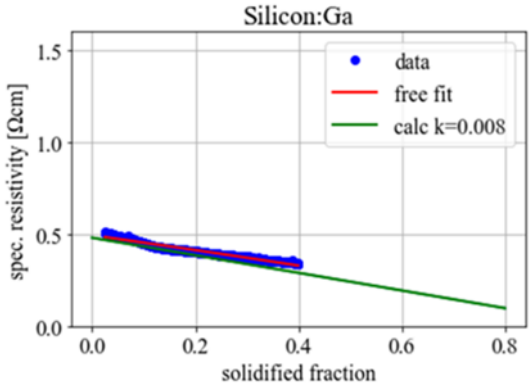

Figure 15: Axial distribution of the specific resistivity in a Ga-doped silicon crystal versus the solidified fraction

From the axial resistivity distributions (Fig.13 - Fig.15), the corresponding concentrations in the melt C_l were estimated according to eq.(6) with the drift mobilities given in Tab.II.

$$C_l = \left(\frac{1}{e\ \mu_D\ \rho\ k}\right) \quad (6)$$

with e: elementary charge, μ_D: drift mobility, ρ: specific resistivity, k: segregation coefficient.

Figs. 16 – 18 show the gallium concentrations in the melt volume corresponding to the solidified fraction. The green curves show the concentrations according to Scheil eq.(4) without evaporation and the weighed amount of dopant

Cl(0) at the start of solidification. The red concentration curves were fitted to the measured data (blue symbols) according to the extended Scheil equation eq.(5). The fit parameters are the initial concentrations in the melt at the beginning of the body phase Cl(0) and the term (γfit/v), where v is the growth rate of 1 mm/min corresponding to the applied average pulling speed.

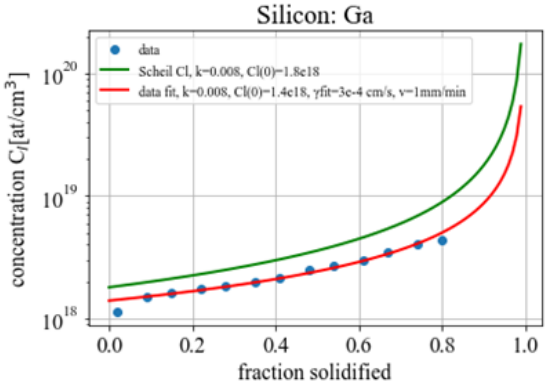

Figure 16: Gallium concentration in the melt versus the solidified fraction

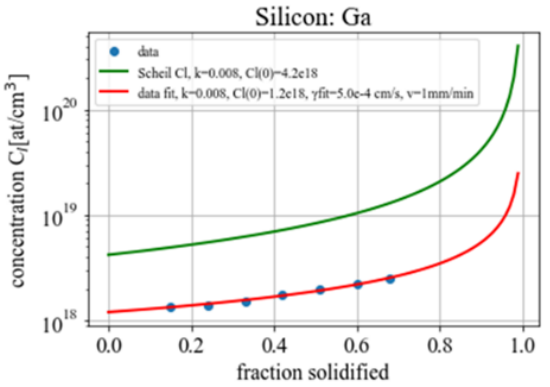

Figure 17: Gallium concentration in the melt versus the solidified fraction

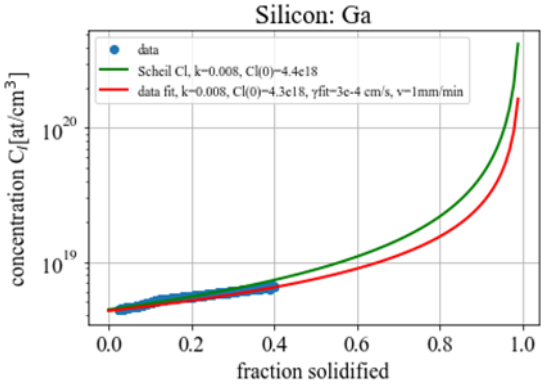

Figure 18: Gallium concentration in the melt versus the solidified fraction, the data points correspond to 1200 as cut wafers

The deviation of the calculated Ga-concentrations without the effect of evaporation (green curves) and the fitted concentrations (red curves) according to eq.(5) is a result of the duration of the time after the melting process and the final start of the body phase. During this period, the volatile dopant may evaporate, depending on the applied process conditions.

The gallium loss due to evaporation can be estimated according to eq.(7) with $\lambda = \gamma$ A/V:

$$C(t) = C(0)e^{-\lambda t} \quad (7)$$

Here, t is the time that elapses after the melting phase to the start of the final body phase. Tab.II summarizes the data for the calculation of the concentration losses according to eq.(7). An average evaporation coefficient of $3.5*10^{-5}$ was applied. The estimated values for the examples of Fig.16 and Fig.18 agree well with the initial values from the fit calculations (see legend). The initial concentration of Fig.17 is significantly below the calculated value, which may be due to the unfavorable A/V ratio.

The evaporation coefficients γ_{fit} obtained from the least square fit calculations (see legend in Figs 16-18) are an order of magnitude higher than the measured evaporation rates. They have to be regarded as pure fitting parameters of the measured values for the evaluation of the totality of the process parameters.

Table III: Data used for calculation of eq. 7

Si:Ga	C(0) [at/cm^3]	A/V [cm^{-1}]	γ [cm/s]	λ=γA/V [s^{-1}]	t [s]	C(t) [at/cm^3]
Fig.16	$1.8*10^{18}$	0.07	$3.5*10^{-5}$	$2.5*10^{-6}$	87000	$1.5*10^{18}$
Fig.17	$4.2*10^{18}$	0.18	$3.5*10^{-5}$	$6.3*10^{-6}$	70000	$2.7*10^{18}$
Fig.18	$4.4*10^{18}$	0.1	$3.5*10^{-5}$	$3.5*10^{-6}$	36000	$3.9*10^{18}$

2.4 Electrical characterization of the investigated samples

For electrical characterization, Hall effect samples were prepared adjacent to the samples for chemical analysis. For the evaluation of the measurement a Hall constant of r = 0.72 was applied, which allows a correct determination of the drift mobility and carrier concentration [7].

$$p = \frac{r}{qR_H} \quad (8)$$

The Hall coefficient R_H is measured experimentally, p is the free hole concentration and r is the hall factor.

Tab.IV summarizes the results of the Hall effect measurements and the chemical content of gallium in the examined samples.

Table IV: Comparison of electronic transport properties with measured gallium concentrations

Ga-conc. [at/cm^3]	4.00E+16	2.72E+16	3.36E+16	2.55E+16
p-conc. [at/cm^3]	3.00E+16	2.52E+16	3.00E+16	2.00E+16
μ drift [cm^2/Vs]	354	360	413	440
μ Hall = $R_H\sigma$ [cm^2/Vs]	255	259	297	317
[p]/[Ga]$_{chem}$	0.77	0.91	0.89	0.78

2.5 Discussion of the measurement results (ICP-MS and Hall effect)

We have calculated the temperature dependent free carrier concentration by numerical solution of the charge-balance equation eq.(9) in weakly compensated p-type silicon for some group III elements.

$$n + N_A^- = p + N_D^+ \quad (9)$$

with n free electron concentration in the conduction band, p free hole concentration in the valence band ,N_A^- concentration of ionized acceptors, N_D^+ concentration of ionized donors.

For the calculation of the different group III elements, an acceptor concentration of N_A=2*10^{16} at/cm^3 and a donor concentration of N_D=5*10^{14} at/cm^3 were assumed. Tab.V summarizes the energy levels for the group III elements used in the charge-balance equation and the calculated degree of ionization. Fig.19 shows the calculated temperature dependent hole concentration for the different elements. The degree of ionization measured in the samples by means of Hall effect and ICP-MS is given in Tab.IV. The ratio p/[Ga]$_{chem}$ includes compensation effects that could not be taken into account in the free hole concentration [p]. The phosphorus and oxygen concentrations were therefore also measured on comparable sample material. With the very low oxygen concentration in the analyzed samples (3-4*10^{17} at/cm^3), no thermal donors acting as compensation centers should be present. The phosphorus concentration was in the range of 10^{14} at/cm^3 and should therefore only contribute insignificantly to the compensation.
Since the energy level of the gallium acceptor in Si is somewhat deeper in the band gap than the boron acceptor, only about 94 % of the substitutionally incorporated Ga has emitted holes into the valence band at 300 K (Tab. V). This fact cannot explain the degree of ionization [p]/[Ga]$_{chem}$ estimated in the examined samples (Tab.IV). It can be stated that in the studied concentration range of gallium in Cz-silicon monocrystals, a significant fraction is not ionized which is confirmed by Hoshikawa et al. [8]. In order to make reliable statements, a systematic investigation on more samples would be necessary. The unionized Ga-atoms should occupy interstitial sites, as they are not electrically active. The extent to which they influence the drift mobility as neutral-impurity scatter centers is unclear.
The fact that only an undefined fraction of the gallium is electrically active affects the determination of the dopant concentration from the measured resistivity data according to eq.(6). Thus, two effects overlap that make a reproducible adjustment of the specific resistivity in Ga-doped Cz-crystals difficult, namely the evaporation of the gallium and the undefined degree of ionization.

Table V: Energy level and degree of ionization of group III elements at room temperature

acceptor	energy level [eV]	degree of ionization @ 300 K [%]
boron	0.045	98
aluminum	0.067	95
gallium	0.072	94
indium	0.16	49

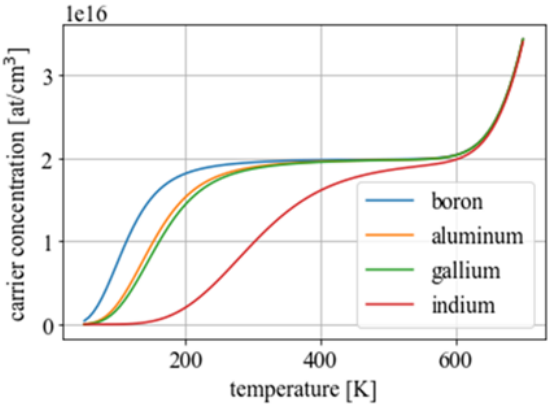

Figure 19: Temperature dependent hole concentration for the group III elements

3 SUMMARY

- Literature values for evaporation rates during the Czochralski process are hardly available and given without sufficient background information.
- During the melting process, only insignificant amount of gallium seems to evaporate.
- Evaporation rates were determined under different process conditions but without a growing crystal.
- The process pressure has a noticeable influence on the evaporation behavior of gallium.
- Since noticeable evaporation of gallium was measured in silicon melt and during growth, participation of oxygen from the silica crucible seems to be involved in the evaporation process.
- The evaporation behavior was determined using an approximate equation with two fit parameters for the different process conditions.
- Under the process conditions studied in this paper, a noticeable fraction of the gallium is apparently incorporated electrically inactive on interstitial site.

4 APPENDIX

Eq.(9b) shows the charge-balance equation of a semiconductor with an acceptor and a donor impurity in detail.

$$N_C exp\left(\frac{E_F - E_C}{kT}\right) + N_A \frac{1}{1 + 4exp\left(\frac{E_A - E_F}{kT}\right)} = N_V exp\left(\frac{E_V - E_F}{kT}\right) + N_D \frac{1}{1 + 2exp(E_F - E_D)} \quad (9b)$$

$N_{C,V}$: effective density of states in the conduction and valence band, $E_{C,V}$: energy of the conduction and valence band edge, E_F: Fermi energy, N_A,N_D: concentration of acceptor and donor atoms, k: Boltzmann-constant, T: absolute temperature.

4 ACKNOWLEDGEMENTS

This work was supported by the German Federal Ministry for Economy Affairs and Climate Action under contract number 03EE1126B

5 REFERENCES

[1] Joyce Ann T. De Guzmann et al., Defect Reactions Responsible for Boron-Oxygen Degradation in Crystalline Silicon Photovoltaics, Proceedings of the 37th EU PVSEC (2020), 145

[2] Joyce Ann T. De Guzmann et al., Indium-Doped Silicon for Solar Cells – Light-Induced Degradation and Deep-Level Traps, Phys. Status Solidi A, **2021**, 218, 2100108

[3] Takeshi Hoshikawa, Toshinori Taishi, Shuji Oishi, Keigo Hoshikawa, Investigation of methods for doping CZ silicon with gallium, Journal of Crystal Growth, 275 (2005) e2141 – e2145

[4] Jafar Safarian, Merete Tangstad, Vacuum refining of molten silicon, Metallurgical and Materials Transactions B, Vol. 43B, 2012, 1427-1445

[5] M. Porrini, R. Scala and V.V. Voronkov, Behavior of Volatile Dopants (P, Sb) in Czochralski Silicon Growth, Journal of Crystal Growth 460, 13-15 (2017).

[6] Zhensheng Liu, Torbjörn Carlberg, A Model for Dopant Concentration in Czochralski Silicon Melts, J. Electrochem. Soc., Vol. 140, No. 7, July 1993, 2052-2057

[7] Blood-Orton "the electrical characterization of semiconductors: majority carriers and electron states", 1992; Fig. 3.14, p. 127; ISBN 0-12-528627-9

[8] Takeshi Hoshikawa et al., Relationship between Gallium Concentration and resistivity of Gallium-doped Czochralski Silicon crystals: Investigation of a conversion curve, Japanese Journal of Applied Physics, Vol. 47, No. 12 2008, pp 8691 – 8695

[9] S.M. Sze, Semiconductor devices, ISBN 0-471-33372-7

[10] Frank Szmulowicz, Calculation oft he mobility and the Hall factor for doped p-type silicon, Physical Review B **34,6** (1986) 4031-4047